ES Materials & Manufacturing

RESEARCH PAPER View Article Online

Enhanced Electrochemical Performance of Cu^{2+} doped TiO_2 Nanoparticles for Lithium-ion Battery

Xiao-Chong Zhao,[1] Pan Yang,[1] Li-Jun Yang,[1] Yu Cheng,[1,3] Hui-Yuan Chen,[3] Hu Liu,[4,5] Gang Wang,[2,*] Vignesh Murugadoss,[4,6] Subramania Angaiah[6,*] and Zhanhu Guo[4,*]

TiO_2 nanoparticles doped with Cu^{2+} are synthesized via a facile one-step solvothermal method with a uniform distribution of 50-60nm. The X-ray photoelectron spectroscopy (XPS) results show that the Cu^{2+} are doped in the TiO_2 crystal lattice uniformly. Due to the smooth replacement of the part of Ti^{4+} sites by Cu^{2+} in the samples, more Ti^{4+} vacancies are formed, which is a benefit to the Li^+ diffusion and enhanced electrochemical properties. At the 5 C rate, the initial discharge capacity of TiO_2 doped with 6 wt% Cu^{2+} reaches 83.4 $mAhg^{-1}$. After 100 charge-discharge cycles, the discharge capacity is still 76.5 $mAhg^{-1}$, showing a good cycling stability.

Keywords: Cu^{2+} doping; TiO_2; Electrochemical Performance; Lithium-ion Battery

Received 4 September 2018, **Accepted** 7 October 2018

DOI: 10.30919/esmm5f109

1. Introduction

Lithium-ion batteries (LIBs) have been widely used in portable electronic devices due to their superior properties such as high energy density, long cycle life, no memory effect and environmental friendliness.[1-4] With rising interest in green electrode materials for LIBs, increasing attention has been paid to titanium dioxide (TiO_2) anode material in recent years because of its long cycle life, low cost, and minimum environmental impact.[5-9] Furthermore, the lithium insertion/extraction voltage of a TiO_2 anode vs. Li+ /Li reaches 1.5 V, which can effectively avoid the formation of solid electrolyte interfaces (SEI) layers and lithium plating on the anode, and improve the safety of the batteries as compared with its carbon-based counterparts.[10,11] However, TiO_2 is also suffering from inherent drawbacks as a potential anode material in LIBs, such as the low ionic diffusivity, poor electronic conductivity in electrodes, and high resistance at the interface of electrode/electrolyte at high charge/discharge rates.[12,13]

To address these issues, a series of strategies have been developed to improve the structural integrity and electrical conductivity of TiO_2-based materials, such as optimizing particle size distribution or surface morphology,[14-17] and fabricating TiO_2/carbon hybrids.[18-20] Minella M et al synthesized titanium dioxide/reduced graphene oxide (TiO_2-rGO) composites at different loadings of the carbonaceous phase and focus on the simplicity and low cost of the electrode production.[13] Yu W et al synthesized anatase TiO_2 ultra-thin nanosheets by a facile hydrothermal method, which exhibited an excellent cycling performance.[11]

In this study, we have presented a facile one-step solvothermal method, which is based on the idea of increasing diffusion channel of Li^+, for the synthesis of TiO_2 nanoparticles doped with Cu^{2+}. The effects of the Cu^{2+} doping on the structure, morphology and surface area of the TiO_2 samples are investigated in detail. Furthermore, the Li^+ diffusion in the LIBs during charge/discharge process is characterized by electrochemical measurements. Due to the uniform replacement of the part of Ti^{4+} sites by Cu^{2+}, more Ti^{4+} vacancies are formed, which is a benefit to the Li^+ diffusion.

2. Experimental Details

2.1 Synthesis of TiO_2 nanoparticles doped with Cu^{2+}.

All materials were used as received without further purification. Tetrabutyl titanate, isopropanol, hydrofluoric acid (HF, 40 wt%), $CuCl_2$. $2H_2O$ were purchased from Sigma-Aldrich.

Firstly, 30 ml of analytically pure isopropanol was taken in a 50ml polytetrafluoroethylene container. Secondly, a required quantity of $CuCl_2.2H_2O$ powder (The Cu^{2+}: Ti^{4+} mass ratio was

[1]*Institute of Materials, China Academy of Engineering Physics, Mianyang 621908, Sichuan, China*
[2]*Institute of Chemical Engineering, Qinghai University, Xining 810016, China*
[3]*Qinghai Nationalities University, Xining 810007, China*
[4]*Integrated Composites Laboratory (ICL), Department of Chemical and Biomolecular Engineering, University of Tennessee, Knoxville, TN 37996 USA*
[5]*National Engineering Research Center for Advanced Polymer Processing Technology, Zhengzhou University, Zhengzhou 450002, China*
[6]*Electrochemical Energy Research Lab, Centre for Nanoscience and Technology,Pondicherry University, Puducherry – 605 014*
***E-mail:** wanggang5208@163.com; a.subramania@gmail.com; zguo10@utk.edu*

controlled as 0, 6 wt%, 9 wt%, 12 wt%, corresponding to the samples of S-0, S-6wt%, S-9wt%, S-12wt%) was added to it. Thirdly, 5 ml tetrabutyl titanate was dropped into the above mixture with continuous magnetic stirring for 10 min. Finally, 0.6 ml HF was added dropwise into the above mixture.

After a solvothermal reaction in an oven for 6 h at 180 °C, the resulting precipitate consisting of TiO_2 nanoparticles doped with Cu^{2+} was washed with distilled water and ethyl alcohol for three times, separately. After sintering at 500 °C for 2 h in an argon atmosphere, the TiO_2 nanoparticles doped with Cu^{2+} were obtained.

2.2 Cell assembly

N-methyl-2-pyrrolidone (NMP, Aldrich) based slurry of the as-prepared doped with Cu^{2+} doped TiO_2 nanoparticles was mixed with acetylene black (Shawinigan Black AB50, Chevron Corp., USA) as electronic conduction enhancer and poly-(vinylidene fluoride) as binder (PVDF, Solvay Solef-6020), in the weight ratio of 80 : 10 : 10. The mixture was then deposited over a copper foil current collector using a standard "doctor blade" technique. After the evaporation of the solvent, the film was hot pressed (10 minutes at 70 °C and 200 bar) in order to improve the adhesion, cut into disks and outgassed, then transferred into an Ar-filled dry glove-box (MBraun Labstar, H_2O and O_2 content <1 ppm) for cell assembly. The electrode loading density of active materials is about 1.1 mg/cm^2. Three-electrode T-cells were assembled by contacting in sequence the working electrode (having the above described composition), a 1.0 M lithium perchlorate ($LiClO_4$, Aldrich) in a 1:1 v/v% mixture of ethylene carbonate (EC, Fluka) and diethyl carbonate (DMC, Aldrich) electrolyte soaked on a polypropylene separator (2400, Celgard) and a lithium foil (high purity lithium foils, Chemetall Foote corporation) counter electrode.

2.3 Characterization and Electrochemical Measurement

The X-Ray Diffraction (XRD) was characterized by TD-3500, Dandong Tongda, China. The scanning electron microscope (SEM) was characterized by S5200, Hitachi, Japan. The surface area and pore size distribution were characterized by QUADRASORB2QDS-evo, Quantachrome Instruments, America. The X-ray photoelectron spectroscopy (XPS) was characterized by ESCALAB 250 XI, Thermo Scientific, America. The CT2001a cell test instrument (LAND Electronic Co.) was used to test the galvanostatic discharge/charge cycling performance of cells in a potential range of 1.0 to 3.0 V (vs. Li/Li$^+$) at 25 ^{0}C. The cyclic voltammetry (CV) and electrochemical impedance spectrum (EIS) characterization were carried out using a Solartron 1470E electrochemistry workstation.

3. Results and Discussion

Phase composition and purity of the samples are characterized by XRD as shown in Fig. 1. The pattern is obviously the same with that standard spectrum of anatase TiO_2, and all the peaks can be well assigned to the TiO_2 ((JCPDS NO.21-1272, I41/amd, a=b=3.7845Å, c =9.5143Å). This indicates that the as-prepared material has good crystallinity and high purity. When the Cu^{2+} doping amount is less than ≤9wt%, the XRD patterns have no indications of other crystalline derivatives, such as CuO or Cu_2O, indicating that the Cu^{2+} is doped into the TiO_2 lattice completely. Meanwhile, the obvious (004) peak reveals the wide existence of highly active (001) plane. The (001) plane of anatase TiO_2 exposure can improve the Li^+ diffusion coefficient, which is conducive to the fast charge/discharge process. However, when the Cu^{2+} doping amount reaches 12wt%, there is another extra peak appearing, which is corresponding to the peak of CuO (JCPDS NO.02-1042).[11]

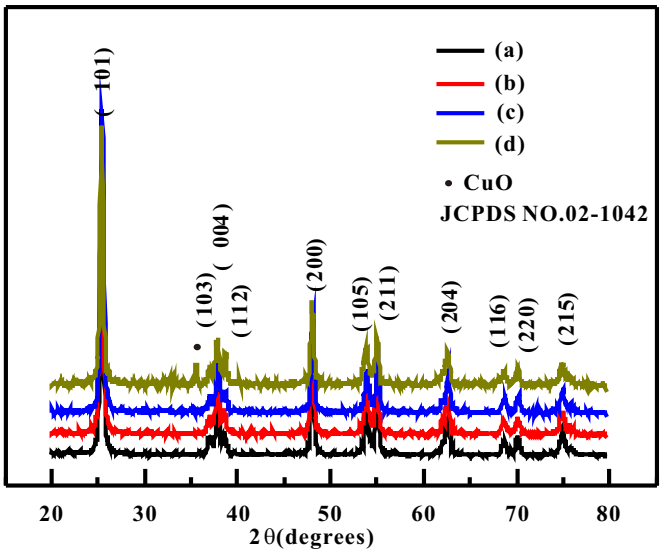

Fig. 1 XRD pattern of samples (a) S-0 (b) S-6wt% (c) S-9wt% (d) S-12wt%.

Fig. 2 presents the morphological results characterized by SEM. The as-prepared samples show a relatively uniform distribution of 50-60nm. The nanoparticles trend a kind of progressive changing process from circular to square. This is consistent with the appearance of (004) plane in the XRD pattern. The SEM results indicate the Cu^{2+} doping has no obvious effects on the anatase TiO_2 morphology. Meanwhile, the specific surface areas of the samples, (a) S-0 (b) S-6wt% (c) S-9wt% (d) S-12wt% are 38.2 m^2 g^{-1}, 35.2 m^2 g^{-1}, 33.8 m^2 g^{-1}, 31.9 m^2 g^{-1}, respectively, showing a typically decreasing trend with the increasing Cu^{2+} doping.[12,13]

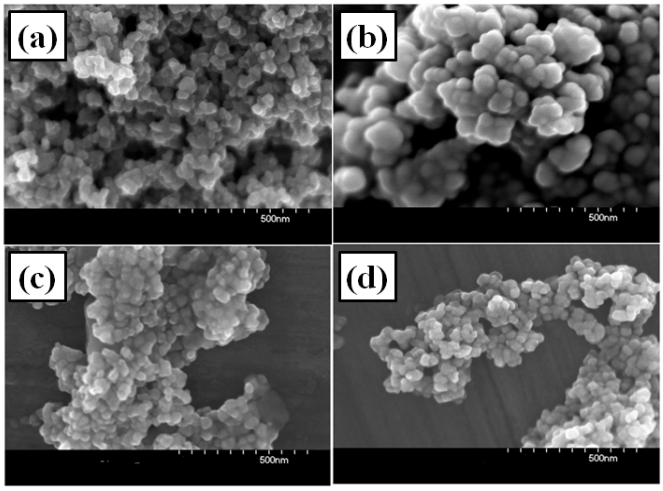

Fig. 2 SEM image of samples (a) S-0 (b) S-6wt% (c) S-9wt% (d) S-12wt%.

Fig. 3 presents the XPS energy spectrum of samples with 6wt% Cu^{2+} doping, full spectrum (a), O peak (b), Ti peak (c) and Cu peak (d), as well as the element mapping spectra of O (e), Ti (f) and Cu (g). The two peaks at 458.7 and 464.5 eV in Fig. 3c correspond to

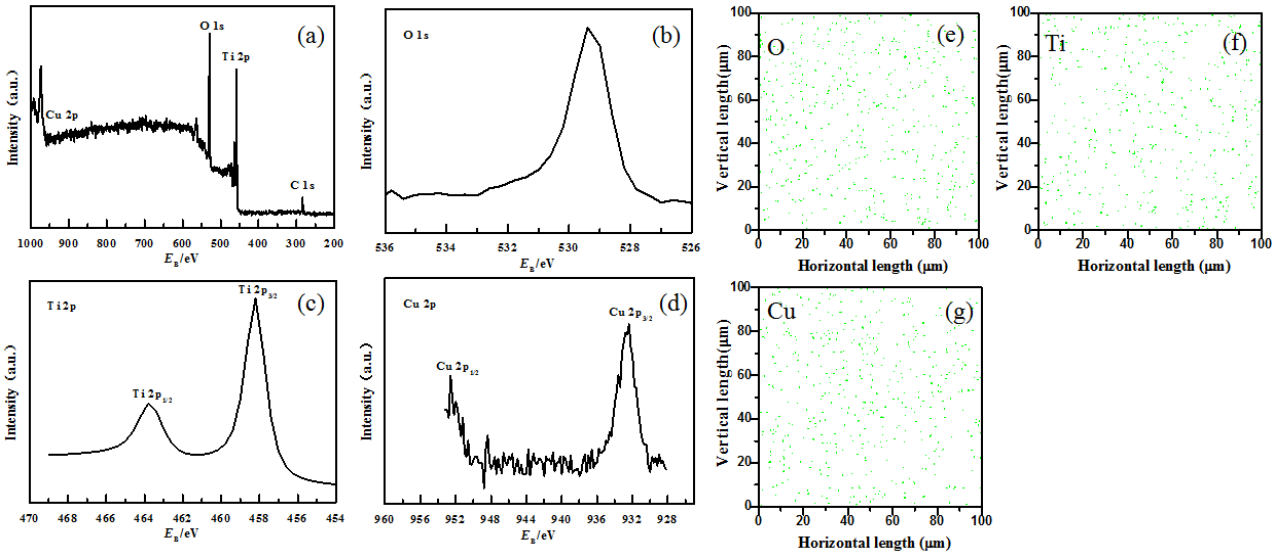

Fig. 3 (a) XPS spectra of S-6wt%, (b) O1s, (c) Ti2p, (d) Cu2p, and elemental mapping of (e) O, (f) Ti & (g) Cu.

the $Ti2p_{3/2}$ and $Ti2p_{1/2}$ states divided from the Ti2p spin-orbit interaction energy. However, these $Ti2p_{3/2}$ and $Ti2p_{1/2}$ peaks shifted from the respective 459.2 and 464.7 eV peaks of pure TiO_2 reported elsewhere,[21,22] which possibly due to the greater number of oxygen vacancies in Cu^{2+} doped TiO_2. This increment in the oxygen vacancies can contribute to electrical conductivity and thereby the enhanced electrochemical performance.[23] The O1s spectrum reveals that the oxygen element exists in the form of O-Ti. Meanwhile, the electron binding energy of $Cu2p_{3/2}$ and $Cu2p_{1/2}$ is 932.1eV and 952.0eV, separately. These are consistent with the binding energy of Cu^{2+}.[24] From the mapping results of Fig. 3 e , f , and g , the O, Ti and Cu show a very uniform distribution, indicating that the Cu^{2+} is doped into the lattice of TiO_2 uniformly.[14]

Fig. 4 presents the initial charge/discharge curves of samples measured at a rate of 0.5C. The initial discharge capacity for the samples of S-0, S-6 wt%, S-9 wt%, and S-12 wt% reaches 151.2, 156.5, 173.8, 138.2 $mAhg^{-1}$, separately. The higher initial discharge capacity of the S-9wt% may due to their relatively higher electronic conductivity as evidenced in Fig. 6, which results in rapid charge transport and a lower electrochemical polarization. These are also consistent with the trend that proper doping of Cu^{2+} is beneficial to improve the specific capacity.[18,19]

To examine the rate performance and cyclic stability, the charge capacity at the 5C rate was investigated for 100 cycles as shown in Fig. 5. The samples of S-0, S-6 wt%, S-9 wt%, and S-12 wt% show initial discharge specific capacity of 76.3, 83.4, 69.4, 79.1 mAh g^{-1}. The initial capacity discharge decreased by 46.7% and 60.06% for S-6 wt% and S-9 wt% at 5C compared to 0.5C, respectively, indicating that the S-6 wt% is more suitable for higher current. This probably results from the comparatively larger volume change as well as copper ion dissolution of S-9 wt% during charge-discharge cycle at higher currents.[25] After 100 cycles, the capacity gradually dropped to 67.5, 76.5, 69.2, 60.2

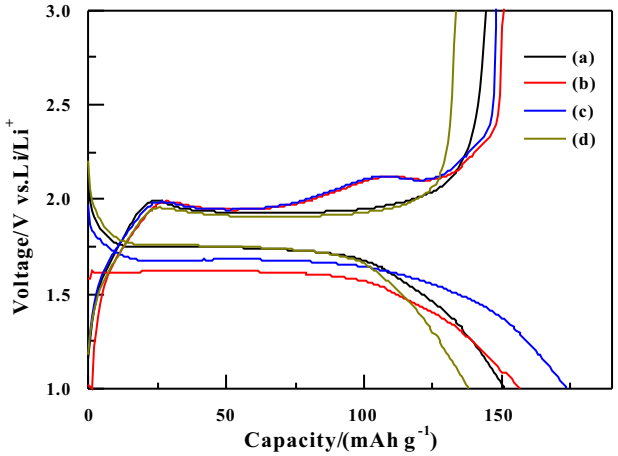

Fig. 4 Initial discharge-charge curves of samples (a) S-0 (b) S-6 wt% © S-9 wt% (d) S-12 wt% at 0.5C rate .

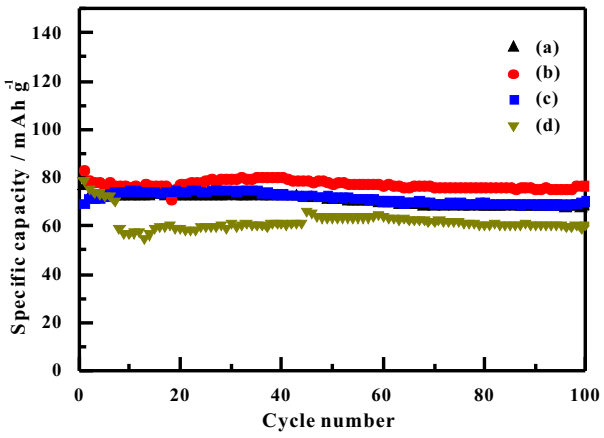

Fig. 5 Charge capacity as a function of cycle number at the 5C rate. (a) S-0 (b) S-6 wt% © S-9 wt% (d) S-12 wt%.

mAhg^{-1}, respectively. The Cu^{2+} doped TiO_2 exhibit superior cyclic stability, implies their excellent structural stability during the lithium de-intercalation/intercalation process. These results refer that proper doping of Cu^{2+} can improve the rate performance and cycle stability obviously. Because the replacement from Ti^{4+} to Cu^{2+} in TiO_2 lattice during the doping, more Ti^{4+} vacancies are formed, increasing the Li^+ diffusion coefficient as well as benefiting the fast Li^+ charge/discharge process. However, when the Cu^{2+} doping amount reaches 12 wt%, CuO appears as shown in Figure 1, which can decrease the conductivity of as-prepared samples. Furthermore, during the cycling process, the volume effect of CuO reaches about 170%, which may cause decreasing electrochemical properties seriously.

Fig. 6 presents the electrochemical impedance spectroscopy (EIS) results for the samples of S-0, S-6 wt%, S-9 wt%, and S-12 wt% after 100 cycles. The respective equivalent circuit is shown in the inset of Fig. 6. All these EIS curves are composed of one semicircle and one straight line. The semicircle in the high-frequency range is consistent with the charge transfer process, responding to the charge transfer impedance (R_{ct}). The smaller the diameter of the semicircle, representing lower R_{ct}, the better the electrochemical properties of as-prepared samples. The line in low-frequency range responds to Li^+ diffusion process in the active material, responding to the Warburg impedance. It can be seen that the samples of S-6 wt% and S-9 wt% with proper Cu^{2+} doping, show a lower R_{ct} compared to that of pure TiO_2 samples. This is consistent with the initial charge/discharge curves as shown in Fig. 4 and Fig. 5. However, when more Cu^{2+} are doped into TiO_2, the samples of S-12 wt% show a R_{ct} equivalent pure TiO_2 samples. That is because too much of Cu^{2+} doping cause the formation of CuO phase, which decreases the conductivity of active materials.[24]

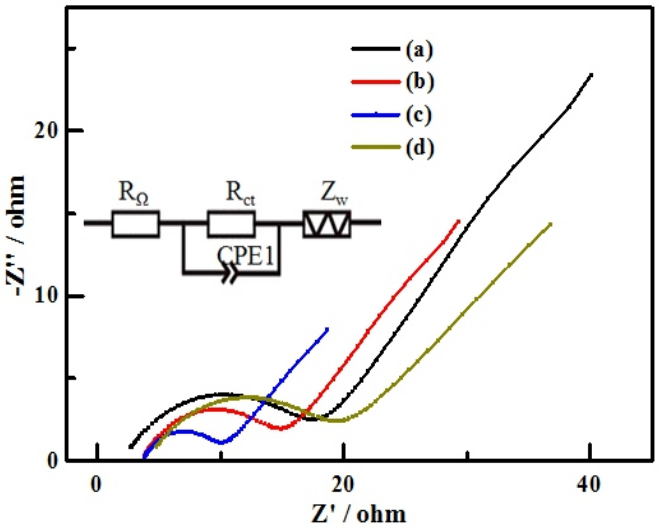

Fig. 6 The EIS spectra after 100 cycles; (a) S-0 (b) S-6 wt% © S-9 wt% (d) S-12 wt%. Inset: A Respective equivalent circuit for fitting.

To better elucidate the electrochemical mechanism of the Cu^{2+} doped anatase TiO_2 nanoparticles, the cyclic voltammogram (CV) in the range between 1.0 and 3.0 V are analyzed and the result is displayed in Fig. 7. In the cycle, a pair of reduction/oxidation peaks at 1.68/2.09 V belong to the Li^+ insertion/extraction processes between TiO_2 and $Li_{0.5}TiO_2$. When the Cu^{2+} doping amount is proper for the samples of S-6wt% and S-9wt%, the peak current densities become higher than that of S-0. Meanwhile, the redox peaks become narrower. Both the higher current density and narrower redox peak indicate that the conductivity becomes better for the samples of S-6 wt% and S-9 wt%. The positions of the redox peaks almost remain unchanged in the 5th cycles, revealing the enhanced cyclability. When the Cu^{2+} doping amount is 12 wt%, the peak current densities decrease to that of S-0. The appearance of CuO in the as-prepared samples results in the decreasing reactive activity. Furthermore, the redox peaks move to keep away from each other. This infers that the electrode polarization happens with the appearance of CuO.[20,24]

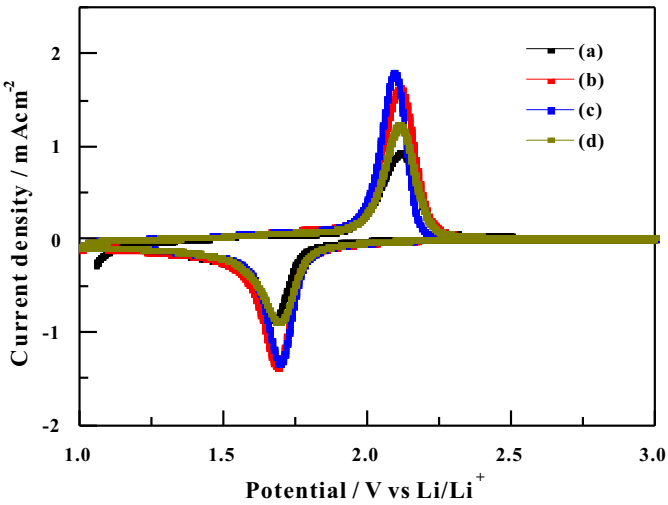

Fig. 7 Cyclic voltammetry of samples (a) S-0 (b) S-6wt% (c) S-9wt% (d) S-12 wt% at a scanning rate of 0.2 mV s^{-1}.

4. Conclusions

A facile one-step solvothermal method is deployed to synthesize TiO_2 nanoparticles doped with different content of Cu^{2+}. The XPS results show that Cu^{2+} is doped in TiO_2 crystal lattice uniformly. At the rate of 5C, the initial discharge capacity of samples doped with 6 wt% Cu^{2+} reached 83.4 mAhg^{-1}. After 100 charge-discharge cycles, the discharge capacity is still 76.5 mAhg^{-1}, showing good cycling stability. Because of the replacement from Ti^{4+} to Cu^{2+} in TiO_2 lattice during the doping, more Ti^{4+} vacancy is formed, increasing the Li^+ diffusion coefficient as well as benefiting the fast Li^+ charge/discharge process. All these efforts result in enhanced electrochemical properties.

Acknowledgements

The authors express their gratitude for the support provided by the Qinghai International Cooperation Project (No. 2014-HZ-816), National Natural Science Foundation of China (NSFC No. 51402267 and 51508484) and the State Key Laboratory of New Ceramic and Fine Processing Tsinghua University (KF201715) for providing financial support.

Conflict of Interest

Authors declare no conflict of interest

References

1. R. Mo, Z. Lei, K. Sun and D. Rooney, *Adv. Mater.*, 2013, **26**, 2084-2088.
2. H. Lyu, P. Li, J. Liu, S. Mahurin, J. Chen, D. K. Hensley, G. M. Veith, Z. Guo, S. Dai and X.-G. Sun, *ChemSusChem*, 2018, **11**, 763-772.
3. X. Lou, C. Lin, Q. Luo, J. Zhao, B. Wang, J. Li, Q. Shao, X. Guo,

N. Wang and Z. Guo, *ChemElectroChem*, 2017, **4**, 3171-3180.
4. J. Guan, Y. Li, Y. Guo, R. Su, G. Gao, H. Song, H. Yuan, B. Liang and Z. Guo, *ACS Sustainable Chem. Eng.*, 2017, **5**, 1026-1032.
5. Z. Wang, M. Liu, G. Wei, P. Han, X. Zhao, J. Liu, Y. Zhou and J. Zhang, *Appl. Surf. Sci.*, 2017, **423**, 375-382.
6. T. Huang, J. Lu, R. Xiao, Q. Wu and W. Yang, *Appl. Surf. Sci.*, 2017, **403**, 584-589.
7. J. Li, H. Cui, X. Song, N. Wei and J. Tian, *Appl. Surf. Sci.*, 2017, **396**, 1539-1545.
8. Y. Hui, L. Qi, Z. Ding, W. Zheng-De, L. Yun-Ying, W. Xiao-Xia and Z. Tie-Yong, *J. Inorg. Mater.*, 2016, **31**, 1242-1248.
9. C. Yu, W. Yan-Zhi and C. Zhao-Fan, *J. Inorg. Mater.*, 2015, **30**, 1218-1222.
10. J. John, B. Gangaja, S. V. Nair and D. Santhanagopalan, *Electrochim. Acta*, 2017, **235**, 191-199.
11. W. Yu, Y. Liu, N. Cheng, B. Cai, K. K. Kondamareddy, S. Kong, S. Xu, W. Liu and X.-Z. Zhao, *Electrochim. Acta*, 2016, **220**, 398-404.
12. Q. Tian, J. Chen, Z. Zhang and L. Yang, *Electrochim. Acta*, 2017, **231**, 670-676.
13. M. Minella, D. Versaci, S. Casino, F. Di Lupo, C. Minero, A. Battiato, N. Penazzi and S. Bodoardo, *Electrochim. Acta*, 2017, **230**, 132-140.
14. G. Armstrong, A. R. Armstrong, J. Canales and P. G. Bruce, *Chem. Commun.*, 2005, 2454-2456.
15. A. R. Armstrong, G. Armstrong, J. Canales and P. G. Bruce, *Angew. Chem., Int. Ed.*, 2004, **43**, 2286-2288.
16. X. Tong, M. Zeng, J. Li and F. Li, *Appl. Surf. Sci.*, 2017, **392**, 897-903.
17. M. Han and G. Chen, *Appl. Surf. Sci.*, 2016, **388**, 401-405.
18. L.-f. Que, F.-d. Yu, Z.-b. Wang and D.-m. Gu, *Electrochim. Acta*, 2016, **222**, 27-35.
19. G. Liu, X. Liu, L. Wang, J. Ma, H. Xie, X. Ji, J. Guo and R. Zhang, *Electrochim. Acta*, 2016, **222**, 1103-1111.
20. H. M. Ren, Y. H. Ding, F. H. Chang, X. He, J. Q. Feng, C. F. Wang, Y. Jiang and P. Zhang, *Appl. Surf. Sci.*, 2012, **263**, 54-57.
21. S. O. Saied, J. L. Sullivan, T. Choudhury and C. G. Pearce, *Vacuum*, 1988, **38**, 917-922.
22. M. Murata, K. Wakino and S. Ikeda, *J. Electron Spectrosc. Relat. Phenom.*, 1975, **6**, 459-464.
23. T. Xia, W. Zhang, J. Murowchick, G. Liu and X. Chen, *Nano Lett.*, 2013, **13**, 5289-5296.
24. M. V. Koudriachova, N. M. Harrison and S. W. de Leeuw, *Phys. Rev. B*, 2002, **65**, 235423.
25. J. He, F. Long, Z. Zou, W. Wang and Z. Fu*, Ionics,* 2015, **21**, 995-1001.